


Cite this: *RSC Adv.*, 2017, 7, 25650

Loading of Co_3O_4 onto Pt-modified nitrogen-doped TiO_2 nanocomposites promotes photocatalytic hydrogen production†

Wen-Dong Wei, Xiang-Yu Liu, Shi-Cong Cui* and Jin-Gang Liu *

Photocatalytic water splitting has been considered as one of the most promising methods to produce hydrogen as a source of clean fuel. Use of co-catalysts and elemental doping in TiO_2 has been extensively explored for effective photocatalysis. Here we report the synthesis of visible light responsive Pt and Co_3O_4 co-modified nitrogen-doped TiO_2 (N- TiO_2) nanocomposites for efficient photocatalytic hydrogen production. Pt- Co_3O_4 (S)/N- TiO_2 (PCNT(S)) and Pt- Co_3O_4 (D)/N- TiO_2 (PCNT(D)) composites were synthesized by one- and two-step methods, respectively. Experimental results showed that additional loading of Co_3O_4 onto a very low content (0.02 wt%) Pt-modified N- TiO_2 nanocomposite significantly increases the efficiency of photocatalytic hydrogen production. Catalyst composites prepared by the two-step method, where close interaction occurred between the surface-loaded Co_3O_4 and Pt on the N- TiO_2 nanoparticles, showed much higher photocatalytic activity for hydrogen production than that prepared by the one-step method, where Co_3O_4 is evenly dispersed in N- TiO_2 . The position of the co-catalyst Co_3O_4 in TiO_2 has a significant effect on the photocatalytic properties of the prepared photocatalysts.

Received 19th March 2017

Accepted 5th May 2017

DOI: 10.1039/c7ra03216a

rsc.li/rsc-advances

1 Introduction

Nowadays, cleaner renewable energy production has become the most prevailing global issue owing to the growing demand for nonrenewable fossil fuels and the environmental pollution caused by these fossil fuels.¹ Recently, hydrogen (H_2), as a secondary source of energy, has been proved to be a promising fuel and energy carrier owing to its renewability, no pollution, ideal calorific value, and universal element properties.^{2–5} Photocatalytic water splitting has been considered as one of the most promising methods to produce H_2 because of its environmentally benign process and the use of solar energy as an energy source.^{6–8} The process was originally discovered by Fujishima and Honda in 1972 through photoelectrochemical water splitting by TiO_2 single crystal electrodes under ultraviolet (UV) light radiation.⁹ Since then, TiO_2 has drawn immense attraction of researchers to water splitting by photoelectrochemical or photocatalytic systems.¹⁰

Nevertheless, the large bandgap (3.2 eV) and high photo-generated electron-hole recombination rate constrain the practical use of TiO_2 in the H_2 evolution reaction.^{11,12} Elemental

doping is an effective way to decrease the semiconductor bandgap.^{13–15} Nitrogen-doped (N-doped) TiO_2 has widely been used in photocatalytic water splitting, which showed efficient H_2 production under visible light irradiation by narrowing the bandgap energy of TiO_2 .^{16,17} At the same time, application of co-catalyst was found to be effective in reducing the recombination of photo generated electron and holes.^{18,19} Thus far, many studies have reported that loading of noble metals such as Au,^{20,21} Ag,²² Pt,²³ and Rh²⁴ on the surface of a semiconductor as a co-catalyst plays an important role in photocatalytic water splitting, which revealed that high H_2 production is due to the electron trapping properties of noble metals. Application of Pt has been extensively studied because an appropriate Schottky barrier is found in it, which is beneficial for H^+ reduction.^{25–27} Yu *et al.*²⁸ fabricated Pt/ TiO_2 by the photochemical reduction of H_2PtCl_6 on TiO_2 and found that the rate of photocatalytic H_2 production was significantly enhanced by loading Pt on the surface of TiO_2 , and the optimal content of Pt loading was about 2.0 wt%. In addition to noble metals, cobalt oxide has recently been explored as an alternative co-catalyst for photocatalytic H_2 production.^{29,30} Bala *et al.*³¹ synthesized the $\text{Co}_3\text{O}_4/\text{TiO}_2$ composite using Co(II) metal-organic frameworks as a TiO_2 absorbent and sacrificial template, in which Co_3O_4 acted as a co-catalyst to extract the photogenerated charge carrier, exhibiting high H_2 evolution rate. However, to the best of our knowledge, no example has been reported about the synergistic effect of different co-catalysts on the H_2 evolution rate of related TiO_2 -based photocatalysts.

Key Laboratory for Advanced Materials, School of Chemistry & Molecular Engineering, East China University of Science and Technology, Shanghai 200237, P. R. China.
E-mail: shicongcui@ecust.edu.cn; liujingang@ecust.edu.cn

† Electronic supplementary information (ESI) available: TEM images of other samples, data of photocatalytic water splitting, and BET of surface areas of all samples. See DOI: 10.1039/c7ra03216a



In this study, we have used two different methods to prepare Pt and Co_3O_4 co-modified N-doped TiO_2 (N-TiO_2) composites and investigated the H_2 evolution from water photocatalyzed by these composites. Results showed that the presence of Co_3O_4 on very low content Pt-modified N-TiO_2 composite further enhanced the photocatalytic efficiency as compared to the Pt-only-modified composite, Pt@N-TiO_2 . Moreover, the position of the Co_3O_4 particles on the composite has a significant effect on the photocatalytic activity of the catalyst.

2 Experimental methods

2.1 Preparation of N-TiO_2

All chemicals used in this study were of analytical grade and used as received without further purification. In the typical synthetic procedure, tetrabutyltitanate (TBOT, 0.029 mol) was added to 30 mL of isopropanol with magnetic stirring. Then, 40 mL of acetic acid solution ($V_{\text{CH}_3\text{COOH}} : V_{\text{H}_2\text{O}} = 1 : 3$) was added dropwise to the above mixture and kept in an ice bath until a white precipitate was obtained. After stirring the solution continuously for 3 h to complete the hydrolysis, a certain amount of choline was added till the pH of the solution reached 9.0. The precursor was then transferred into a 50 mL Teflon-lined autoclave and heated at 180 °C for 24 h in an oven. Then, it was allowed to cool to room temperature naturally. A yellowish-white precipitate was obtained after centrifuging the solution, and the precipitate was washed several times with water and ethanol and dried at 60 °C overnight. The obtained composite was further annealed at 300 °C for 3 h (2 °C min^{-1}) under air atmosphere to afford N-TiO_2 .

2.2 Preparation of $\text{Co}_3\text{O}_4/\text{N-TiO}_2$

The $\text{Co}_3\text{O}_4/\text{N-TiO}_2$ composites were synthesized by two different methods: two-step and one-step methods. The composites prepared by the two-step method were represented as $\text{Co}_3\text{O}_4(\text{D})/\text{N-TiO}_2$ (CNT(D)). The Co_3O_4 co-catalyst was loaded onto N-TiO_2 through impregnation of aqueous $\text{Co}(\text{NO}_3)_2$ solution on the N-TiO_2 nanoparticles. About 0.5 mL of aqueous $\text{Co}(\text{NO}_3)_2$ solution with different concentrations (25, 62.5, 125, and 312.5 mmol L^{-1}) was slowly added to 0.5 g of N-TiO_2 powder, and the resultant composite was left for several hours till the powder was thoroughly soaked. The impregnated powder was dried at 60 °C and calcined under air atmosphere at 300 °C for 3 h (2 °C min^{-1}). In $\text{Co}_3\text{O}_4/\text{N-TiO}_2$ composites having different concentrations of $\text{Co}(\text{NO}_3)_2$, the molar ratios of Co : Ti atoms were 0.002, 0.005, 0.01, and 0.025, respectively, and they were represented as CNT(D)-1, CNT(D)-2, CNT(D)-3, and CNT(D)-4, respectively.

The $\text{Co}_3\text{O}_4/\text{N-TiO}_2$ composites synthesized by the one-step method were represented as $\text{Co}_3\text{O}_4(\text{S})/\text{N-TiO}_2$ (CNT(S)). First, TBOT (0.029 mol) and different amounts of cobalt nitrate hexahydrate ($\text{Co}(\text{NO}_3)_2 \cdot 6\text{H}_2\text{O}$) were added to 30 mL of isopropanol with constant magnetic stirring. The procedure was the same as that described for the two-step method in Section 2.1. However, the molar ratios of Co : Ti atoms (Co : Ti = 0.002, 0.005, 0.01, and 0.025) were adjusted by controlling the

concentration of $\text{Co}(\text{NO}_3)_2$ solution (25 mM to 0.31 M) during the preparation process. The composites thus prepared were labeled as CNT(S)-1, CNT(S)-2, CNT(S)-3, and CNT(S)-4, respectively.

2.3 Preparation of $\text{Pt-Co}_3\text{O}_4/\text{N-TiO}_2$

The $\text{Pt-Co}_3\text{O}_4/\text{N-TiO}_2$ composites were prepared by *in situ* photoreduction of H_2PtCl_6 on $\text{Co}_3\text{O}_4/\text{N-TiO}_2$ under light irradiation. CNT(S) or CNT(D) powder (1.0 g) was dispersed in a H_2PtCl_6 solution (100 mL, 0.01 mmol L^{-1}) to produce the Pt 0.02 wt% loaded $\text{Co}_3\text{O}_4(\text{S})/\text{N-TiO}_2$ (PCNT(S)) or the Pt 0.02 wt% loaded $\text{Co}_3\text{O}_4(\text{D})/\text{N-TiO}_2$ (PCNT(D)). The different loading amount of Pt in the system was controlled by changing the concentration of the H_2PtCl_6 solution. The resulting suspension was stirred and irradiated by a 300 W Xe arc lamp for 1 h in a top-irradiation cell with a Pyrex window. The composites were then centrifuged and freeze dried.

2.4 Characterizations

The morphology and structure of these composites were analyzed through transmission electron microscopy (TEM) and high-resolution transmission electron microscopy (HRTEM) with a JEOL model JEM 2100 EX instrument at an acceleration voltage of 200 kV. X-ray powder diffraction (XRD) was performed with a Rigaku Dmax-3C diffractometer using Cu K α radiation ($\lambda = 0.15408 \text{ nm}$) operated at 40 kV and 20 mA to characterize the crystal phases and crystallinity of the samples. Ultraviolet-visible (UV-Vis) absorption spectra of the samples were recorded by a Shimadzu UV-2600 spectrophotometer at a wavelength of 1000–200 nm. The photoluminescence (PL) spectra were measured using a fluorospectrophotometer (Horiba Fluoromax-4) at room temperature. The chemical states of surface elements were analyzed by X-ray photoelectron spectroscopy (XPS; Perkin-Elmer PHI 5000C).

2.5 Photocatalytic hydrogen production

During water splitting for the evolution of H_2 , photocatalytic activity was evaluated under visible light and full spectrum irradiation. Photocatalytic experiments were performed in a gas-closed system using a Pyrex cell with a top quartz window. Typically, 100 mg of photocatalyst powder was ultrasonically dispersed in 100 mL of aqueous solution containing methanol as a sacrificial agent ($V_{\text{H}_2\text{O}} : V_{\text{MeOH}} = 9 : 1$). Before irradiation, the system was evacuated several times to remove the residual air completely and then irradiated from the top window using a 300 W Xe lamp and a UV light cutoff filter ($\lambda > 400 \text{ nm}$) with a light intensity of 380 mW cm^{-2} . The reaction temperature was maintained at 25 °C with a water cooling circulator. The reaction was performed for 6 h, and the H_2 gas produced was analyzed by a gas chromatograph (SHIMADZU GC-2014) equipped with a thermal conductivity detector. The sample of the gaseous mixture (2.0 mL) was drawn from the online sampling loop and argon was used as the carrier gas. Control experiments were performed without and with photocatalysts under light irradiation and in the dark, respectively.



3 Results and discussions

3.1 Morphologies and structures

The micromorphology and structures of the catalysts PCNT(D)-2 and PCNT(S)-2 with best photocatalytic performance were analyzed by TEM and HRTEM. In Fig. 1a, PCNT(D)-2 was shown with TiO₂ nanoparticles that have an average diameter of 17 nm. There were also other small particles attached to the TiO₂ nanoparticles, indicating the presence of Co₃O₄ on the surface of TiO₂. Fig. 1b displayed the HRTEM image of PCNT(D)-2. A lattice spacing of 0.35 nm matched well with the (101) crystal plane of anatase TiO₂. Moreover, a lattice fringe of 0.24 nm indicated that the bare crystal of (311) plane over Co₃O₄ emerged,³² revealing the successful loading of Co₃O₄. When Pt-Co₃O₄/N-TiO₂ was prepared by the one-step method, an average particle diameter of 12 nm ranging from 9 to 16 nm were obtained, which may be due to the disturbance of Co during the formation of TiO₂. A lattice spacing of 0.37 nm corresponded to anatase TiO₂ (101) crystal plane (Fig. 1d).^{33,34} No other crystal was found in the HRTEM image of PCNT(S)-2, indicating that Co₃O₄ were probably dispersed in the N-TiO₂ particles rather than loaded onto the surface of N-TiO₂. No Pt particle was found in either sample, suggesting the low content of Pt in the composites.

3.2 XRD analysis

With the help of XRD measurements, the crystal phases of the samples were evaluated. Fig. 2a displayed the XRD patterns of PCNT(D). In the case of N-TiO₂, all the diffraction peaks around $2\theta = 25.28^\circ, 37.80^\circ, 48.05^\circ, 53.89^\circ, 55.06^\circ, 62.69^\circ, 68.76^\circ, 70.31^\circ$, and 75.03° were attributed to (101), (004), (200), (105), (211), (204), (116), (220), and (215) crystal planes of anatase TiO₂ (JCPDS card no. 21-1272),^{35,36} respectively. Different from N-TiO₂, a small portion of anatase TiO₂ began to transfer to brookite TiO₂ when 0.002 of Co was introduced. The diffraction peaks at $30.81^\circ, 36.25^\circ$, and 40.15° , which were in accordance with (121), (012),

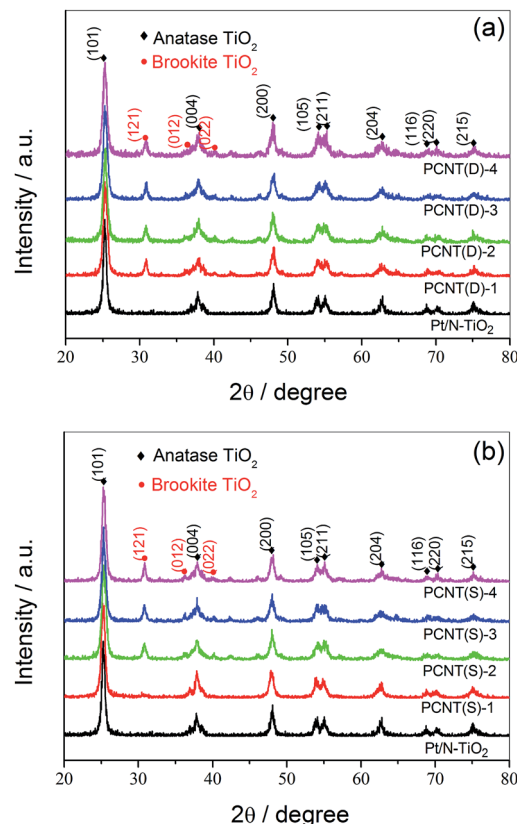


Fig. 2 X-ray powder diffraction patterns of PCNT(D) (a) and PCNT(S) (b).

and (022) lattice planes of brookite TiO₂, respectively, confirmed the existence of brookite.³⁷ As shown in Fig. 2b, no brookite TiO₂ was observed till the amount of Co was about 0.005 in PCNT(S) (PCNT(S)-2), which was different from that of PCNT(D). By increasing the Co content from 0.002 to 0.005, brookite was found in TiO₂, indicating the co-existence of both anatase and brookite TiO₂. The presence of Co₃O₄ probably affects the rearrangement of the atoms in TiO₂ thus promoting anatase to brookite transformation during the crystal formation process. This phenomenon has also been found in other publications.^{38,39} It was reported that TiO₂ mixture containing both anatase and brookite revealed excellent thermal stability, which might be a valuable factor for the high efficiency of photocatalytic water splitting.⁴⁰ Moreover, no typical diffraction peaks assignable to Pt- and Co-based components were detected, which may be because of their low content.

3.3 UV-Vis diffuse reflectance spectroscopy analysis

The optical properties of the samples were investigated by UV-Vis diffuse reflectance spectroscopy (DRS), and the corresponding bandgap energies (E_g) were estimated by the Kubelka-Munk plots.⁴¹ Fig. 3a shows the DRS spectra of N-TiO₂, Pt/N-TiO₂ and PCNT(D), from which we could observe that N-TiO₂ exhibited slight visible light absorption. After loading Co₃O₄ to N-TiO₂, the absorption of the PCNT(D) composites in visible region further increased. The composites showed prominent

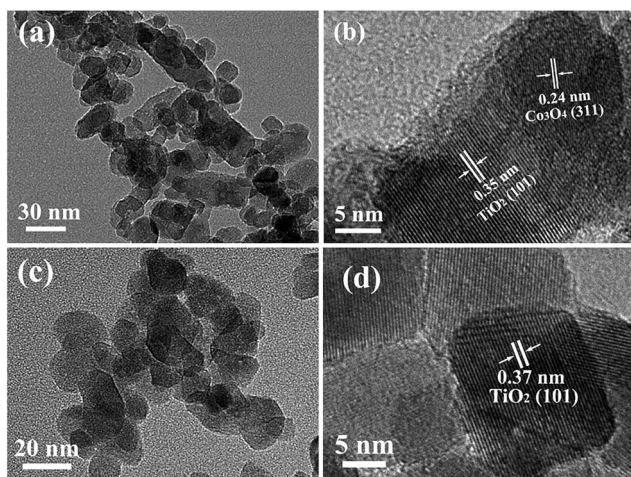


Fig. 1 Transmission electron microscope and high-resolution transmission electron microscopic images of PCNT(D)-2 (a and b) and PCNT(S)-2 (c and d).



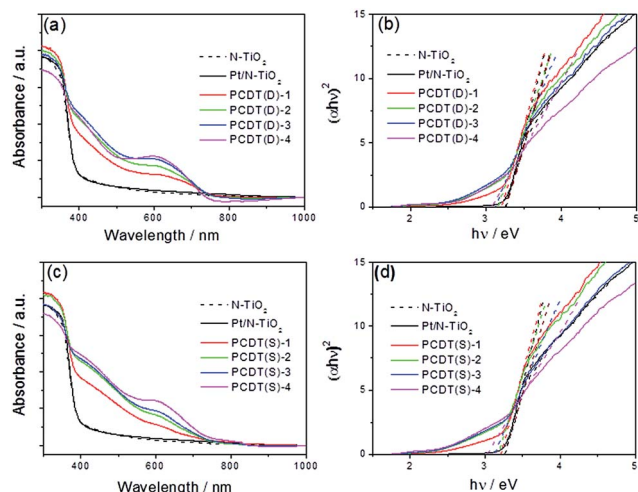


Fig. 3 Ultraviolet-visible (UV-Vis) diffuse reflectance spectra (a and c) and the corresponding Kubelka–Munk plots (b and d) of PCNT(D) (a and b) and PCNT(S) (c and d) with different amounts of Co₃O₄.

light absorption in the range of 400–700 nm, which was mainly attributed to the $\text{O}^{2-} \rightarrow \text{Co}^{3+}$ and $\text{O}^{2-} \rightarrow \text{Co}^{2+}$ transitions of loaded Co₃O₄ that has small band gaps.^{42,43} With the increase of Co content, the absorption intensity increased gradually, particularly in the region from 500 to 700 nm. The E_g values of TiO₂ in Pt/N-TiO₂, PCNT(D)-1, PCNT(D)-2, PCNT(D)-3, and PCNT(D)-4 were estimated to be 3.26, 3.21, 3.16, 3.13, and 3.08 eV, respectively (Fig. 3b). The samples prepared by two-step method showed similar UV-Vis absorption as that prepared by the one-step method (Fig. 3c). As shown in Fig. 3d, the E_g values of TiO₂ in N-TiO₂, PCNT(S)-1, PCNT(S)-2, PCNT(S)-3, and PCNT(S)-4 were 3.26, 3.21, 3.17, 3.12, and 3.02 eV, respectively. Obviously, loading Co₃O₄ to the composite promotes the catalyst for higher visible light absorption. This would beneficially contribute to the photo-activity of the composite under visible light irradiation. While, it should be noted that the catalyst composite with the best catalytic activity is not the one with the most visible light absorption as observed in this study for the H₂ production. Similar phenomena have also been reported by other researchers.^{44,45}

3.4 PL behavior

The photocatalytic activity of photocatalysts is usually closely associated with the separation and recombination behavior of the photogenerated electrons and holes.^{46,47} PL spectra of PCNT(D) and PCNT(S) with different amounts of Co were then measured. From Fig. 4a and b, it was obvious that the PL intensities of PCNT(D) and PCNT(S) were significantly smaller than that of Pt/N-TiO₂. For the PCNT catalyst composites, the photogenerated electrons in the conduction band of N-TiO₂ could transfer into the energy level of modified Co₃O₄, which may reduce the radiative recombination efficiency of photo-generated electrons and holes. This indicates that loading Co₃O₄ on the catalyst composite separates the photogenerated charge carriers effectively, which is beneficial for the photocatalytic activity.

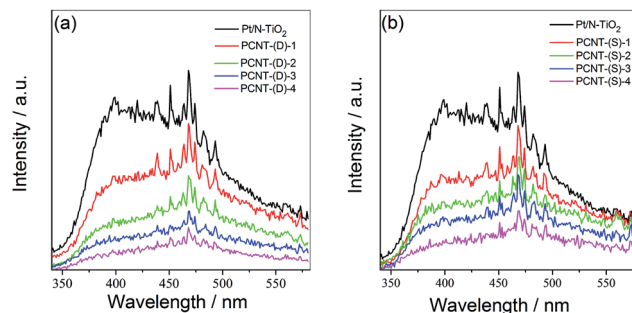


Fig. 4 Photoluminescence (PL) spectra of PCNT(D) (a) and PCNT(S) (b) with different Co contents.

3.5 XPS analysis

XPS spectra were measured to investigate the surface chemical components and chemical states of the samples. Fig. 5 showed the XPS spectra of Pt/N-TiO₂, PCNT(D)-2, and PCNT(S)-2. In Fig. 5a, the XPS survey spectra showed that Pt/N-TiO₂ contained Ti, O, N, and Pt elements, whereas both PCNT(D)-2 and PCNT(S)-2 contained Ti, O, N, Pt, and Co elements due to the introduction of Co. High-resolution XPS spectra of Pt 4f and Co 2p were shown in Fig. 5b and c, respectively. The Pt 4f band of Pt/N-TiO₂ and PCNT(S)-2 was divided into two Gaussian–Lorentzian peaks with binding energies at around 74.9 and 76.8 eV, respectively, corresponding to metallic (Pt⁰) Pt 4f_{7/2} and 4f_{5/2} states.⁴⁸ The blue shifts of the Pt peaks in PCNT(D)-2 (74.4 and 75.7 eV) and PCNT(S)-2 (75.0 and 76.5 eV) were compared (Fig. 5b). This could be attributed to the interaction of Co in Co₃O₄ with Pt on the surface of PCNT(D)-2. As shown in Fig. 5c, Co was detected in both PCNT(D)-2 and PCNT(S)-2. The peaks of Co in PCNT(D)-2 were found at approximate 780.8 and 795.7 eV which were assignable to the binding energies of Co 2p_{3/2} and 2p_{1/2}.⁴⁹ While the binding energies for Co in PCNT(D)-2 were found at about 783.3 and 796.6 eV, which shifted to higher energy relative to PCNT(S)-2, suggesting the interaction between Co₃O₄ and Pt.⁵⁰

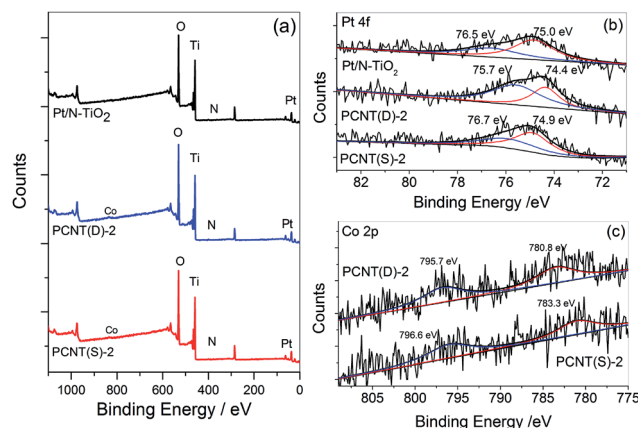


Fig. 5 X-ray photoelectron spectra (XPS) of Pt/N-TiO₂, PCNT(D)-2, and PCNT(S)-2 for survey (a), Pt 4f (b), and Co 2p (c).

XPS etching was then employed to explore the existence of Co in PCNT(D)-2 and PCNT(S)-2. The Co contents on the surface and 5 nm inside PCNT(D)-2 were 2.39 and 2.01 at%, respectively. The larger content of Co on the surface than that in the interior could be ascribed to the additional loading of Co_3O_4 on the surface of N-TiO₂. On the other hand, in the case of PCNT(S)-2, both values were essentially the same, 1.02 and 1.03 at%, respectively. The XPS etching results indicated that Co_3O_4 was evenly dispersed in N-TiO₂ when prepared by the one-step method, but it was mainly loaded on the surface of N-TiO₂ when synthesized by the two-step method.

3.6 Water splitting activity

The effects of Pt loading amount on the H₂ evolution rate of CNT(D)-2 and CNT(S)-2 under UV-Vis and visible light irradiation were shown in Fig. 6. The H₂ evolution rates of CNT(D)-2 and CNT(S)-2 under UV-Vis light varied with the Pt-loading amount. It was clearly shown that additional loading of Co_3O_4 onto appropriate amount of Pt modified N-TiO₂ composite remarkably improved the photocatalytic efficiency for H₂ production (Fig. 6a, Table S1†), which signifies the important contribution from the loaded Co_3O_4 . It is interesting to note that CNT(D)-2 exhibited higher H₂ evolution rates in all cases than CNT(S)-2. The maximum differences of H₂ production rates were obtained with a Pt loading of 0.02 wt% in both CNT(D)-2 and CNT(S)-2, which revealed the optimal concentration of Pt loading. With Pt loading higher than 0.02 wt%, the rate of H₂ evolution declined quickly at 0.2 wt%. The same trend was observed when the samples were irradiated under visible light (Fig. 6b, Table S2†). The higher catalytic activity of CNT(D)-2 than CNT(S)-2 could be attributed to the synergistic effect played by the closely contacted Pt with Co_3O_4 on the surface of N-TiO₂.

The effect of Co contents on the photocatalytic performance of PCNT(D) and PCNT(S) was then investigated. Fig. 7a showed the H₂ evolution rate of PCNT(D) and PCNT(S) with different Co contents under visible light irradiation ($\lambda > 400$ nm). It was clear that the H₂ evolution rate of PCNT(D) increased with the increase in Co contents from 0.002 to 0.005 and then decreased with further increase in Co content to 0.025. The H₂ evolution rate achieved a maximum value of $197 \mu\text{mol g}^{-1} \text{h}^{-1}$ at 0.005 content, suggesting optimal Co content. In addition, it was noteworthy that when Co content increased to 0.025, the H₂ evolution rate rapidly decreased to $32 \mu\text{mol g}^{-1} \text{h}^{-1}$. The extremely low

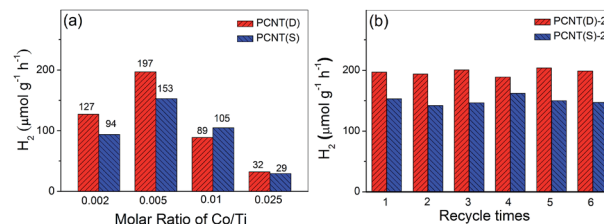


Fig. 7 Photocatalytic H₂ evolution of PCNT(D) and PCNT(S) versus different amounts of Co (a), and photocatalytic H₂ evolution in six-run recycling experiments using PCNT(D)-2, and PCNT(S)-2 composites (b).

H₂ production was probably due to the formation of vast crystal defects, which greatly promoted the recombination of photoelectrons and holes. A similar trend was observed in PCNT(S) samples with different Co contents, in which Co content at 0.005 showed the highest H₂ evolution (Fig. 7a, Table S3†). The stability of the photocatalysts was investigated by a six-run recycling experiment of H₂ evolution under similar conditions. PCNT(D) showed higher photocatalytic activities as compared to PCNT(S). As shown in Fig. 7b, after six-run cycles, H₂ evolution, catalyzed by PCNT(D) and PCNT(S), mainly remained as high as the initial, suggesting the excellent stabilities of both PCNT(D) and PCNT(S).

Taken all the experimental results together, it can be concluded that loading of Co_3O_4 on Pt/N-TiO₂ composite significantly promotes the PCNT catalysts photocatalytic activity, and PCNT(D) showed much higher H₂ evolution rates than PCNT(S) composites under the same Pt-loading content. This indicates that the existing state of Co_3O_4 in the composites played a crucial role in the photocatalytic performance of the catalyst. XPS spectra and TEM images of the composites showed the distribution of Co_3O_4 in PCNT(D) and PCNT(S), where Co_3O_4 was located on the surface of N-TiO₂ in PCNT(D) (Fig. 8a) and was evenly dispersed in N-TiO₂ in the case of PCNT(S) (Fig. 8b). For the PCNT(D) composites (Fig. 8a), visible light irradiation of N-TiO₂ produces photogenerated electrons and holes; the generated electrons are then captured by the closely contacted Pt/ Co_3O_4 particles on which water splits to produce hydrogen, and the holes were consumed by reacting with the sacrificial donor reagent. In the case of PCNT(S) composites, Co_3O_4 and Pt were

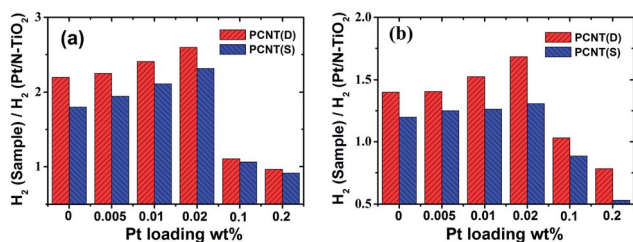


Fig. 6 Effects of different amounts of Pt loading on H₂ evolution rate of PCNT(D) and PCNT(S) under UV-Vis (a) and visible light (b) irradiation, respectively.

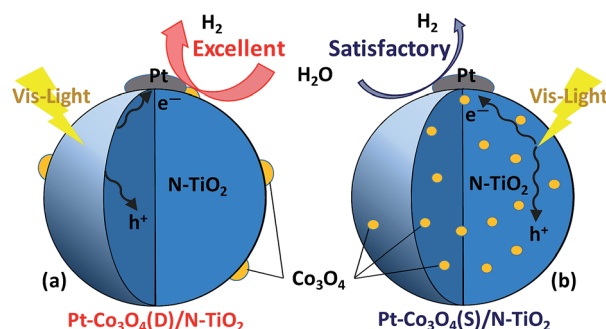


Fig. 8 Pictorial depiction of the existence of Co_3O_4 in PCNT(D) (a) and PCNT(S) (b).



located separately on the surface of N-TiO₂ lacking of direct interaction (Fig. 8b), in which charge separation efficiency would be lower than that in the PCNT(D) composites when photo-irradiated. Accordingly, when appropriate amounts of Co₃O₄ and Pt were loaded onto the surface of N-TiO₂ nanoparticles, the close interaction between Co₃O₄ and Pt may provide more effective electric transmission, showing synergistic effect for promoting the separation of photogenerated electrons and holes and thus boosting the photocatalytic activity.

4 Conclusions

The visible light responsive photocatalysts PCNT(S) and PCNT(D) were synthesized successfully by one-step and two-step methods, respectively. Compared with the Pt@N-TiO₂ catalyst, Co₃O₄-modified composites show significant improvements in the photocatalytic performance for H₂ production with very low loading of Pt (0.02 wt%). Catalyst composites prepared by the two-step method showed higher photocatalytic activity for H₂ production than that prepared by the one-step method. The two-step method led to close interaction between the loaded Co₃O₄ and Pt on the N-TiO₂ nanoparticles, whereas the one-step method produced composites with Co₃O₄ evenly dispersed in N-TiO₂. The methods of preparation and thus the co-catalyst distribution in TiO₂ have a strong influence on the catalytic properties of the prepared composites. The results obtained may have implications for further development of high-performance catalysts for photocatalytic H₂ production.

Acknowledgements

This study was financially supported by the NSF of China (no. 21271072, 21571062 to JGL; 21571063 to SCC), the Program for Professor of Special Appointment (Eastern Scholar) at Shanghai Institutions of Higher Learning to JGL, and the Fundamental Research Funds for the Central Universities (no. 222201717003).

Notes and references

- 1 M. Y. Liu, W. Zhou, T. Wang, D. F. Wang, L. Q. Liu and J. H. Ye, *Chem. Commun.*, 2016, **52**, 4694–4697.
- 2 D. F. Su, J. Wang, H. Y. Jin, Y. T. Gong, M. M. Li, Z. F. Pang and Y. Wang, *J. Mater. Chem. A*, 2015, **3**, 11756–11761.
- 3 M. Z. Ge, C. Y. Cao, S. H. Li, Y. X. Tang, L. N. Wang, N. Qi, J. Y. Huang, K. Q. Zhang, S. S. Al-Deyabe and Y. K. Lai, *Nanoscale*, 2016, **8**, 5226–5234.
- 4 R. Liu, Z. Zheng, J. Spurgeon and X. G. Yang, *Energy Environ. Sci.*, 2014, **7**, 2504–2517.
- 5 M. N. Ha, F. Zhu, Z. F. Liu, L. C. Wang, L. Y. Liu, G. Z. Lu and Z. Zhao, *RSC Adv.*, 2016, **6**, 21111–21118.
- 6 P. A. Bharad, K. Sivarajani and C. S. Gopinath, *Nanoscale*, 2015, **7**, 11206–11215.
- 7 C. Marchal, M. Behr, F. Vigneron, V. Caps and V. Keller, *New J. Chem.*, 2016, **40**, 4428–4435.
- 8 A. Iwase, S. Yoshino, T. Takayama, Y. H. Ng, R. Amal and A. Kudo, *J. Am. Chem. Soc.*, 2016, **138**, 10260–10264.
- 9 A. Fujishima and K. Honda, *Nature*, 1972, **238**, 37–38.
- 10 W. Zhou, W. Li, J. Q. Wang, Y. Qu, Y. Yang, Y. Xie, K. F. Zhang, L. Wang, H. G. Fu and D. Y. Zhao, *J. Am. Chem. Soc.*, 2014, **136**, 9280–9283.
- 11 S. Pany and K. M. Parida, *Phys. Chem. Chem. Phys.*, 2015, **17**, 8070–8077.
- 12 J. Fang, L. Xu, Z. Y. Zhang, Y. P. Yuan, S. W. Cao, Z. Wang, L. S. Yin, Y. S. Liao and C. Xue, *ACS Appl. Mater. Interfaces*, 2013, **5**, 8088–8092.
- 13 X. F. Zhang, B. Y. Zhang, Z. X. Zuo, M. K. Wang and Y. Shen, *J. Mater. Chem. A*, 2015, **3**, 10020–10025.
- 14 X.-Y. Liu, W.-D. Wei, S.-C. Cui and J.-G. Liu, *Catal. Lett.*, 2016, **146**, 1655–1662.
- 15 W. Q. Fang, Z. Y. Huo, P. R. Liu, X. L. Wang, M. Zhang, Y. Jia, H. M. Zhang, H. J. Zhao, H. G. Yang and X. D. Yao, *Chem. – Eur. J.*, 2014, **20**, 11439–11444.
- 16 W. Wang, Y. Liu, J. F. Qu, Y. B. Chen and Z. P. Shao, *RSC Adv.*, 2016, **6**, 40923–40931.
- 17 T. Wang, X. Q. Yan, S. S. Zhao, B. Lin, C. Xue, G. D. Yang, S. J. Ding, B. L. Yang, C. S. Ma, G. Yang and G. R. Yang, *J. Mater. Chem. A*, 2014, **2**, 15611–15619.
- 18 N. Liu, C. Schneider, D. Freitag, U. Venkatesan, V. R. R. Marthala, M. Hartmann, B. Winter, E. Spiecker, A. Osvet, E. M. Zolnhofer, K. Meyer, T. Nakajima, X. M. Zhou and P. Schmuki, *Angew. Chem.*, 2014, **126**, 14425–14429.
- 19 N. Liu, V. Häublein, X. M. Zhou, U. Venkatesan, M. Hartmann, M. Mačković, T. Nakajima, E. Spiecker, A. Osvet, L. Frey and P. Schmuki, *Nano Lett.*, 2015, **15**, 6815–6820.
- 20 R. Reichert, Z. Jusys and R. J. Behm, *J. Phys. Chem. C*, 2015, **119**, 24750–24759.
- 21 A. A. Melvin, K. Illath, T. Das, T. Raja, S. Bhattacharyya and C. S. Gopinath, *Nanoscale*, 2015, **7**, 13477–13488.
- 22 R. Kobayashi, S. Tanigawa, T. Takashima, B. Ohtani and H. Irie, *J. Phys. Chem. C*, 2014, **118**, 22450–22456.
- 23 F. L. Wang, Y. J. Jiang, D. J. Lawes, G. E. Ball, C. F. Zhou, Z. W. Liu and R. Amal, *ACS Catal.*, 2015, **5**, 3924–3931.
- 24 T. Ikeda, A. Xiong, T. Yoshinaga, K. Maeda, K. Domen and T. Teranishi, *J. Phys. Chem. C*, 2013, **117**, 2467–2473.
- 25 B. Banerjee, V. Amoli, A. Maurya, A. K. Sinha and A. Bhaumik, *Nanoscale*, 2015, **7**, 10504–10512.
- 26 P. Chowdhury, G. Malekshoar, M. B. Ray, J. Zhu and A. K. Ray, *Ind. Eng. Chem. Res.*, 2013, **52**, 5023–5029.
- 27 C. L. Muhich, Y. Zhou, A. M. Holder, A. W. Weimer and C. B. Musgrave, *J. Phys. Chem. C*, 2012, **116**, 10138–10149.
- 28 J. G. Yu, L. F. Qi and M. Jaroniec, *J. Phys. Chem. C*, 2010, **114**, 13118–13125.
- 29 G. J. Ai, R. Mo, H. X. Li and J. X. Zhong, *Nanoscale*, 2015, **7**, 6722–6728.
- 30 A. Meng, J. Zhang, D. Xu, B. Cheng and J. Yu, *Appl. Catal., B*, 2016, **198**, 286–294.
- 31 S. Bala, I. Mondal, A. Goswami, U. Pal and R. Mondal, *J. Mater. Chem. A*, 2015, **3**, 20288–20296.
- 32 T. Wang, X. G. Meng, G. G. Liu, K. Chang, P. Li, Q. Kang, L. Q. Liu, M. Li, S. X. Ouyang and J. H. Ye, *J. Mater. Chem. A*, 2015, **3**, 9491–9501.



- 33 S. M. Y. M. Mukthar Ali and K. Y. Sandhya, *RSC Adv.*, 2016, **6**, 60522–60529.
- 34 A. Y. Yermakov, G. S. Zakharova, M. A. Uimin, M. V. Kuznetsov, L. S. Molochnikov, S. F. Konev, A. S. Konev, A. S. Minin, V. V. Mesilov, V. R. Galakhov, A. S. Volegov, A. V. Korolyov, A. F. Gubkin, A. M. Murzakayev, A. D. Syvazhin and K. V. Melanin, *J. Phys. Chem. C*, 2016, **120**, 28857–28866.
- 35 R. Tang, Z. R. Xie, S. J. Zhou, Y. N. Zhang, Z. M. Yuan, L. Y. Zhang and L. W. Yin, *ACS Appl. Mater. Interfaces*, 2016, **8**, 22201–22212.
- 36 Y. J. Li, H. R. Yang, J. Tian, X. L. Hu and H. Z. Cui, *RSC Adv.*, 2017, **7**, 11503–11509.
- 37 A. Zielinska-Jurek, I. Wysocka, M. Janczarek, W. Stampor and J. Hupka, *Sep. Sci. Technol.*, 2015, **156**, 369–378.
- 38 C. Zhao, X. Shu, D. Zhu, S. Wei, Y. Wang, M. Tu and W. Gao, *Superlattices Microstruct.*, 2015, **88**, 32–42.
- 39 R. Jaiswal, N. Patel, A. Dashora, R. Fernandes, M. Yadav, R. Edla, R. S. Varma, D. C. Kothari, B. L. Ahuja and A. Miotello, *Appl. Catal., B*, 2016, **183**, 242–253.
- 40 C. Perego, Y. H. Wang, O. Durupthy, S. Cassaignon, R. Revel and J. P. Jolivet, *ACS Appl. Mater. Interfaces*, 2012, **4**, 752–760.
- 41 L. Zhang, X. H. Huang, J. S. Hu, J. Song and I. Kim, *Langmuir*, 2017, **33**, 1867–1871.
- 42 G. Dai, S. Liua, Y. Liang and T. Luo, *Appl. Surf. Sci.*, 2013, **264**, 157–161.
- 43 T. Wang, X. Meng, G. Liu, K. Chang, P. Li, Q. Kang, L. Liu, M. Li, S. Ouyang and J. Ye, *J. Mater. Chem. A*, 2015, **3**, 9491–9501.
- 44 S. Huang, Y. Yu, Y. Yan, J. Yuan, S. Yin and Y. Cao, *RSC Adv.*, 2016, **6**, 29950–29957.
- 45 S. G. Babu, R. Vinoth, D. P. Kumar, M. V. Shankar, H.-L. Chou, K. Vinodgopal and B. Neppolian, *Nanoscale*, 2015, **7**, 7849–7857.
- 46 J. J. Wu, S. L. Lu, D. H. Ge, L. Z. Zhang, W. Chen and H. W. Gu, *RSC Adv.*, 2016, **6**, 67502–67508.
- 47 P.-P. Sun, L. Liu, S.-C. Cui and J.-G. Liu, *Catal. Lett.*, 2014, **144**, 2107–2113.
- 48 Y. Chang, C. H. Yuan, Y. T. Li, C. Liu, T. Wu, B. Zeng, Y. T. Xu and L. Z. Dai, *J. Mater. Chem. A*, 2017, **5**, 1672–1678.
- 49 B. Huang, W. J. Yang, Y. W. Wen, B. Shan and R. Chen, *ACS Appl. Mater. Interfaces*, 2015, **7**, 422–431.
- 50 D. B. Hamal and K. J. Klabunde, *J. Phys. Chem. C*, 2011, **115**, 17359–17367.

